EJNMMI RESEARCH

ORIGINAL RESEARCH

Open Access

^{68}Ga-NOTA-RM26 PET/CT in the evaluation of glioma: a pilot prospective study

Yilin Li[1,2†], Rongxi Wang[3†], Jingci Chen[4], Zhaohui Zhu[2,3*], Yu Wang[1,2*] and Wenbin Ma[1,2*]

Abstract

Background Gliomas are the most common malignant primary tumors of the central nervous system. There is an urgent need for new convenient, targeted and specific imaging agents for gliomas. This study aimed to firstly evaluate the feasibility of ^{68}Ga-NOTA-RM26 PET/CT imaging in glioma and analyze the relationship between the imaging characteristics and glioma grade, classification and molecular alterations.

Results Twenty-two patients were confirmed as glioma by surgery or biopsy. All patients exhibited ^{68}Ga-NOTA-RM26 uptake. SUV_{max} was chosen as the imaging marker for analysis. For all glioma patients, there were significant differences between grades ($P=0.047$). For primary gliomas, SUV_{max} had good discrimination for both tumor classifications ($P=0.045$) and grades ($P=0.03$). There was a positive correlation ($P<0.01$) between GRPR expression level and SUV_{max}. P53 mutations caused significant differences in SUV_{max} ($P=0.03$).

Conclusions This study is the first application of ^{68}Ga-NOTA-RM26 in glioma patients and confirmed the safety and efficacy in glioma patients. ^{68}Ga-NOTA-RM26 PET/CT has potential value in tumor grade, classification, and molecular alterations.

Trial registration ClinicalTrials.gov: NCT06412952. Registered 26 April 2024, https://clinicaltrials.gov/study/NCT06412952

Keywords Glioma, ^{68}Ga-NOTA-RM26, Gastrin-releasing peptide receptor (GRPR), PET/CT

†Yilin Li and Rongxi Wang have contributed equally to this work.

*Correspondence:
Zhaohui Zhu
13611093752@163.com
Yu Wang
ywang@pumch.cn
Wenbin Ma
mawb2001@hotmail.com
[1] Department of Neurosurgery, Center for Malignant Brain Tumors, National Glioma MDT Alliance, Peking Union Medical College Hospital, Chinese Academy of Medical Sciences and Peking Union Medical College, Beijing 100730, China
[2] Chinese Academy of Medical Sciences and Peking Union Medical College, Beijing 100730, China
[3] Department of Nuclear Medicine, State Key Laboratory of Complex Severe and Rare Diseases, Beijing Key Laboratory of Molecular Targeted Diagnosis and Therapy in Nuclear Medicine, Peking Union Medical College Hospital, Chinese Academy of Medical Sciences and Peking Union Medical College, Beijing 100730, China
[4] Department of Pathology, Peking Union Medical College Hospital, Chinese Academy of Medical Sciences and Peking Union Medical College, Beijing 100730, China

Background

Glioma is the most common primary malignant tumor of the central nervous system [1], According to the fifth edition of the World Health Organization (WHO) Classification of Tumors of the Central Nervous System (CNS), adult-type diffuse gliomas can be classified into glioblastomas, IDH-wildtype, astrogliomas, IDH-mutation, oligodendrogliomas, IDH-mutation and 1p/19q-codeleted, and others according to their origin and molecular alterations [2]. Glioblastomas are associated with a median survival of 12–15 months, even with aggressive treatment [3, 4].

The diagnosis of gliomas still relies on postoperative pathology. Preoperative imaging information can be non-invasive and the most commonly used technique is magnetic resonance imaging (MRI), which is an anatomical imaging technique. PET functional imaging can reflect the metabolism or receptor expression of the tumor. The most widely used imaging agent in tumors is ^{18}F-FDG(2-^{18}F-fluoro-2-deoxyglucose) [5], but the natural background high uptake in brain tissue makes ^{18}F-FDG application in glioma imaging unsatisfactory [6, 7]. Amino acid-based imaging agents have been widely studied recently, such as ^{11}C-methionine (^{11}C-MET), ^{18}F-fluoroethyl-L-tyrosine (^{18}F-FET), or ^{18}F-dihydroxyphenylalanine (^{18}F-DOPA), showing high uptake in glioma cells, but they are not tumor specific and their nuclides require accelerators for preparation [8, 9]. And the short half-life of carbon-11 (20 min) restricted the use of ^{11}C-MET[10]. When using ^{18}F-DOPA, an increased uptake in the striatum has to be considered, as the molecule is a precursor of dopamine [11]. Other PET tracers visualizing proliferative tumor cell activity (e.g., ^{18}F-fluorothymidine) or cell membrane components (e.g., ^{11}C-choline) are under investigation in gliomas and are not ready for clinical applications at present [12, 13]. The proposal of PET-based response assessment criteria for diffuse gliomas (PET RANO 1.0) indicated that the importance of PET in glioma has been paid more and more attention [14]. Therefore, there is an urgent clinical need of new convenient and target-specific imaging agents for glioma imaging, to enable tumor detection at the molecular level and visualization of tumor biological behavior, while providing potential theranostic targets.

Gastrin-releasing peptide receptor (GRPR), a member of the G protein-coupled receptor family of bombesin receptors, is overexpressed in various types of human tumors, including glioma, prostate cancer, breast cancer, colorectal cancer, pancreatic cancer, and small cell lung cancer [15]. Previous study showed that all specimens from glioma patients were GRPR immunohistochemical staining positive, while GRPR was not detected in glial cells in normal brain tissue [16, 17]. Previous studies have also found that synthetic GRPR antagonists have antiproliferative effects on GBM cells in vitro and in vivo [18, 19]. ^{68}Ga is produced by a generator rather than a cyclotron and the 67.6-min physical half-life is suitable [20]. The GRPR agonist probe ^{68}Ga-NOTA-Aca-BBN (7–14) has been studied in gliomas [21]. However, as an agonist, it has suboptimal pharmacokinetics in vivo and causes side effects in patients due to its physiological activity [22]. Therefore, imaging probes based on GRPR antagonists have been investigated. Recent studies have shown that GRPR antagonists are superior to GRPR agonists, with higher binding capacity and more favorable pharmacokinetics [23]. Several PET tracers based on GRPR antagonists have been clinically investigated, including RM26 (D-Phe-Gln-Trp-Ala-Val-Gly-His-Sta-Leu-NH2), a high affinity GRPR antagonist [24, 25]. Previous researches have shown that ^{68}Ga-NOTA-RM26 PET/CT is safe and useful in both prostate cancer patients and breast cancer patients [26, 27]. However, its application in glioma patients has not been explored.

In this study, we aimed to explore the potential application value of ^{68}Ga-NOTA-RM26 in glioma patients for the first time, and to analyze the relationship between the imaging characteristics and glioma grade, classification and other molecular alterations.

Methods

Patients

This study was registered on ClinicalTrials.gov (NCT06412952). The study protocol was approved by the Ethics Committee of Peking Union Medical College Hospital (ZS-1103) before recruitment, and all patients signed the informed consent. Patients with suspected gliomas or recurrence based on MRI examinations of the head were recruited at Peking Union Medical College Hospital. Inclusion criteria were clinical suspicion of gliomas/recurrence, age $\geq$ 18 years, signed informed consent, and the ability to obtain pathological specimens through surgery or biopsy. Exclusion criteria were severe liver or kidney disease (serum creatinine levels > 3.0 mg/dL or any liver enzyme levels $\geq$ 5 times the upper limit of normal), severe allergy or hypersensitivity reactions to contrast agents, claustrophobia (unable to undergo PET/CT scans), and pregnancy or breastfeeding.

Procedure

The preparation of NOTA-RM26 was conducted according to the method reported in the literature [24]. The radiolabeling of NOTA-RM26 was performed in a sterile hot chamber following previously reported procedures [21]. The radiochemical purity of the product ^{68}Ga-NOTA-RM26 exceeded 95%. All patients received intravenous injection of 1.85 MBq (0.05 mCi) of ^{68}Ga-NOTA-RM26

per kilogram of body weight within 1 week before surgery. Thirty minutes after the injection, all patients voided urine and assumed a supine position with their arms placed at their sides. The ^{68}Ga-NOTA-RM26 PET/CT of the head was acquired using an integrated PET/CT scanner (Polestar m660, SinoUnion Healthcare Inc., Beijing, China). Low-dose CT scans (120 kV, 35 mA, 70 cm field of view) were acquired for imaging of the head. PET scans for each patient covered one bed position (600 s per bed, 192×192 matrix, 5 mm slice). All patients underwent preoperative MRI navigation and histological results were obtained through biopsy or gross resection.

Image and data analysis

PET/CT images were manipulated on MIM software (version 7.1.4; MIM Software Inc.). PET images were analyzed by two experienced nuclear medicine physicians for 10 and 12 years respectively. For ^{68}Ga-NOTA-RM26 PET/CT imaging, PET positivity was defined as focal tracer uptake of the tumor on a local background and anatomically coregistered with MRI. The background uptake area was the brain tissue in the corresponding region contralateral to the tumor. The maximum and mean standardized uptake values (SUV_{max} and SUV_{mean}, respectively) in the volume of interest were obtained by software. The ratio of tumor to background (T/B) was calculated for further analysis.

Immunohistochemical staining of GRPR

Tumor samples were fixed in 10% neutral buffered formalin and embedded in paraffin. After paraffin sections were deparaffinized to water, 4 μm thick tissue sections were placed in 3% hydrogen peroxide solution and incubated at room temperature in the dark for 25 min. The slides were washed 3 times in PBS (Phosphate-Buffered Saline) (PH 7.4) with shaking on a decolorizing shaker for 5 min each time to block endogenous peroxidase. The tissue was uniformly covered by dropping 3% BSA (Bovine Serum Albumin) in the histochemical circle and blocked for 30min at room temperature. In addition, rabbit anti-human GRPR polyclonal antibody (PA5-26791; Thermo Fisher Scientific, 1:100 dilution) were incubated overnight at 4 °C. After washing with PBS (PH 7.4), CY5-labelled goat anti-rabbit IgG (GB27303; Servicebio) was added and incubated warm for 50 min. After washing with PBS (PH 7.4), the staining was developed with DAB, hematoxylin re-staining, hematoxylin differentiation solution, and hematoxylin blueing solution. Optical microscopy (BX41; Olympus) examined stained slides.

To semi-quantify GRPR expression, five high magnification fields of view (×40) containing malignant cell populations were randomly identified on each slide, and the intensity and percentage of GRPR staining were scored. The intensity of staining was scored as (0, no staining; 1, very low; 2, low; 3, moderate; 4 high staining). The percentage of GRPR positivity in tumor cells was scored as follows: 0%, score 0; 0–20%, score 1; 20–40%, score 2; 40–60%, score 3; 60–80%, score 4; and 80–100%, score 5. For each slice, a value known as the H-score was obtained by multiplying the intensity score by the percentage score. This method has previously been shown to be highly reproducible (intra-class correlation analysis of intra-observer and inter-observer differences: $r=0.94$ and $r=0.9$, respectively) [28]. The procedure was performed independently by two examiners with 10 and 12 years of experience who were unaware of the imaging results, and in cases of discrepancies, a third investigator with 20 years of experience will be consulted to provide an interpretation until a consensus is reached by the group.

Other immunohistochemical and molecular alteration assays were performed as required according to clinical routine.

Statistical analysis

SPSS (IBM SPSS Statistics for Windows, Version 27.0.1; Armonk, NY) was used for data analysis, and RStudio (PBC & Certified B Corp.®, USA) was used to generate graphs. All quantitative data were expressed as mean ± standard deviation. A $P<0.05$ was considered statistically significant. Correlations were analyzed using Spearman correlation coefficient for continuous data. Differences were analyzed by Student's t-test between two groups and Analysis of Variance (ANOVA) between multiple groups.

Results

Baseline information

Twenty-three patients were recruited at the Peking Union Medical College Hospital between April 2024 and August 2024. Twenty-two patients were confirmed as glioma by surgery or biopsy. One patient was histologically confirmed to be not glioma after surgery. Among the gliomas, 20 patients underwent surgical resection or biopsy in our hospital and obtained pathology, while 2 patients underwent surgical resection in other hospitals and we subsequently obtained the pathological diagnosis through telephone follow-up. Of the 22 patients with gliomas, 20 were primary gliomas and 2 were recurrent gliomas. The flow chart is shown in Fig. 1. There were 11 females and 11 males with a mean age of 48.86 ± 13.05 years. Among the primary glioma patients, seven (35.00%) patients were diagnosed as glioblastoma, IDH-wildtype, WHO grade 4. One of them had two lesions. Six (30.00%) patients were diagnosed as astrocytoma, IDH-mutation (WHO grade 4, n = 4, WHO grade

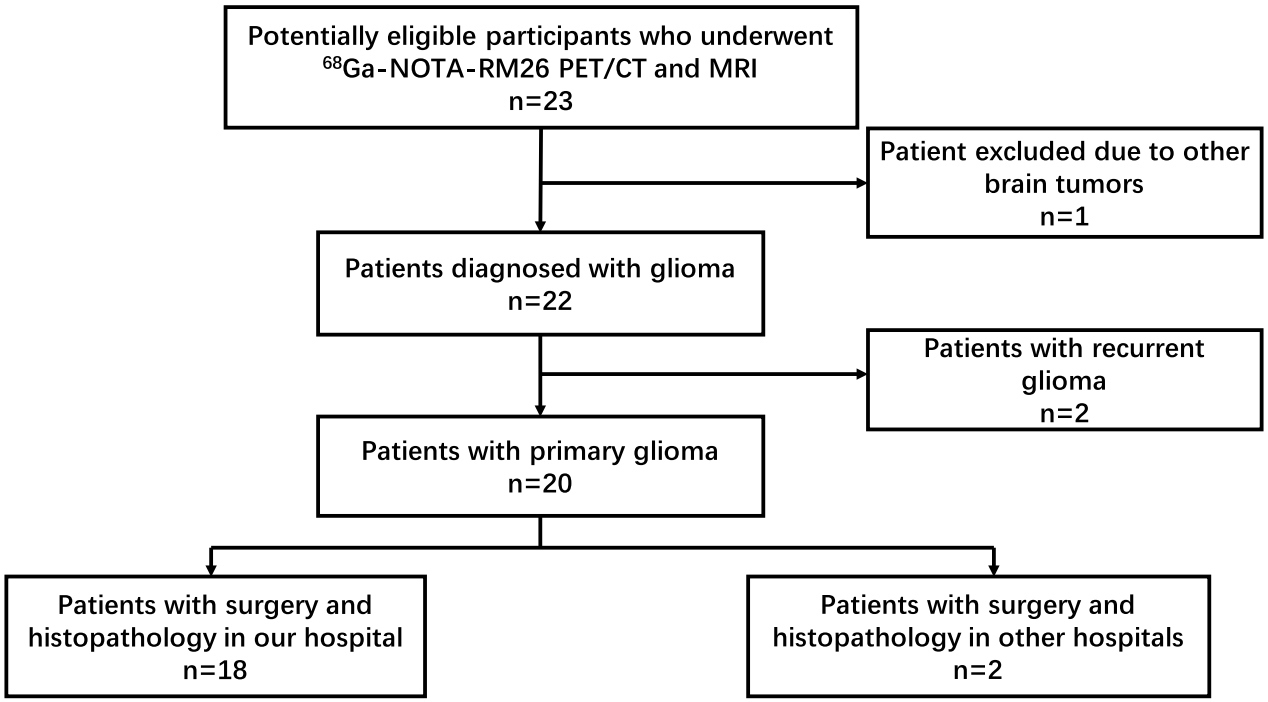

Fig. 1 The flow chart of patient enrollment

3, n = 1, WHO grade 2, n = 1). Four (20.00%) patients were oligodendroglioma, IDH-mutation and 1p/19q-codeleted (WHO grade 3, n = 3, WHO grade 2, n = 1). One patient was diffuse hemispheric high-grade glioma, H3G34 mutant, WHO grade 4. Two patients were diffuse gliomas, WHO grade 2, NOS. Among recurrent gliomas, there was one oligodendroglioma, WHO grade 2 and one glioblastoma. Of all patients, 4 (18.18%) patients were grade 2 gliomas, 4 (18.18%) patients were grade 3, and 14 (63.64%) patients were grade 4. The baseline information of the patients is shown in Table 1.

PET/CT findings

In this study, no significant study-related adverse reactions (dizziness, vomiting, abdominal discomfort) were observed in all patients after ^{68}Ga-NOTA-RM26 administration, indicating that it's well tolerated and safe. All 22 glioma patients showed obvious tracer aggregation in all 23 lesions 30 min after injection of ^{68}Ga-NOTA-RM26, with clear contrast with the surrounding normal brain tissue. The locations of the lesions matched well with the MRI sequences and immunohistochemical results (Fig. 2). The PET/CT image showed glioblastoma in the right frontal lobe, and its location and morphology are basically consistent with MRI. PET/CT uptake can be seen to be slightly larger than the region of enhancement in the T1 + C sequence. The heterogeneity of the uptake intensity within the tumor was observed on PET, while the heterogeneous signals of the tumor were also observed on T1WI, T2WI and T1 + C sequences. They all reflected the heterogeneity within the gliomas. The lesion had a high Ki-67 score, dense tumor cells on HE staining, and a high H-score for GRPR-stained cells. The locations of the lesions for different grades gliomas matched well with the MRI findings (Fig. 3). Shown from top to bottom are gliomas of grade 2, grade 3, and grade 4, respectively. Their PET/CT uptake was enhanced in turn, and the corresponding GRPR staining was also increased. The SUV_{max} of all tumors ranged from 0.10 to 3.40 (1.50 ± 0.47), and the T/B ratio from 2.00 to 35.15 (14.24 ± 0.51).

Correlation between imaging parameters and diagnosis

Different semi-quantitative parameters were further analyzed in this study, including SUV_{max}, SUV_{mean}, T/N_{max}, T/N_{mean}. The Spearman correlation was displayed by heat map (Fig. 4). SUV_{max} was found to be the most representative. So, the subsequent analysis focused on the correlation between SUV_{max} and diagnosis.

For 23 lesions in 22 glioma patients, there was no significant difference in uptake between glioma types ($P = 0.08$, Fig. 5A). Given that glioblastomas are the most malignant and specific, preoperative identification of glioblastomas has some clinical value. We divided them into glioblastoma lesion group (n = 9, SUV_{max} 2.00 ± 0.85) and non-glioblastoma lesion group (n = 14, SUV_{max}

Table 1 Baseline table of patient characteristics

No.	Sex	Age	Diagnosis	Primary	Location	WHO grade	SUVmax	T/B ratio
1	Female	30	Astrocytoma, IDH-mutation, grade 4	Primary	Right temporal lobe	4	1.441	35.146
2	Female	57	Oligodendroglioma, IDH-mutation and 1p/19q-codeleted, grade 3	Primary	Right frontal lobe	3	0.250	3.086
3	Female	60	Oligodendroglioma, IDH-mutation and 1p/19q-codeleted, grade 2	Recurrent	Right frontal lobe	2	2.055	31.136
4	Male	48	Glioblastoma, IDH-wildtype	Primary	Right temporal lobe	4	1.728	23.040
5	Female	58	Astrocytoma, IDH mutation, grade 4	Primary	Left frontal lobe	4	2.640	29.011
6	Female	71	Glioblastoma, IDH-wildtype	Primary	Right frontal lobe	4	0.779	14.164
7	Female	48	Glioblastoma, IDH-wildtype	Primary	Right frontal lobe	4	1.582	16.143
8	Male	51	Diffuse glioma, NOS	Primary	Right frontal lobe	2	1.079	5.832
9	Male	24	Astrocytoma, IDH-mutation, grade 2	Primary	Right frontal lobe	2	0.580	5.225
10	Male	36	Oligodendroglioma, IDH-mutation and 1p/19q-codeleted, grade 2	Primary	Left occipital lobe	2	1.100	11.000
11	Female	51	Astrocytoma, IDH-mutation, grade 3	Primary	Right temporal lobe	3	2.100	18.421
12	Male	69	Glioblastoma, IDH-wildtype	Primary	Left temporal lobe	4	3.400	6.182
			Glioblastoma, IDH-wildtype	Primary	Left temporal lobe	4	2.300	11.500
13	Male	53	Glioblastoma, IDH-wildtype	Recurrent	Left temporal lobe	4	2.440	11.619
14	Female	39	Diffuse glioma, NOS	Primary	Left occipital lobe	2	0.204	2.000
15	Male	42	Astrocytoma, IDH-mutation, grade 4	Primary	Right occipital lobe	4	1.330	12.091
16	Male	49	Oligodendroglioma, IDH-mutation and 1p/19q-codeleted, grade 3	Primary	Right frontal lobe	3	1.130	7.533
17	Female	61	Glioblastoma, IDH-wildtype	Primary	Right frontal lobe	4	2.340	10.685
18	Female	34	Diffuse midline glioma, H3K27-altered	Primary	Left parietal lobe	4	0.940	9.126
19	Female	41	Astrocytoma, IDH-mutation, grade 4	Primary	Right frontal lobe	4	1.575	8.036
20	Male	36	Oligodendroglioma, IDH-mutation and 1p/19q-codeleted, grade 3	Primary	Right parietal lobe	3	0.100	10.000
21	Male	46	Glioblastoma, IDH-wildtype	Primary	Right basal ganglia	4	0.850	12.500
22	Male	71	Glioblastoma, IDH-wildtype	Primary	Right occipital lobe	4	2.595	34.145

1.18 ± 0.76) and found a significant difference between the two (P = 0.03) (Fig. 5B). The optimal cut-off for diagnosis was 1.58, with a sensitivity of 77.8%, specificity of 78.6% and Area Under Curve (AUC) of 0.76 (Fig. 5C). We wondered whether SUV_{max} could preoperatively differentiate primary glioma subtypes. We found that the uptake SUV_{max} of primary glioblastoma lesions (n = 8) was 1.95 ± 0.89, astrocytoma (n = 6) was 1.61 ± 0.70 and oligodendroglioma (n = 4) was 0.65 ± 0.54. It was significantly different among different subgroups (P = 0.045), and the uptake of glioblastoma was significantly higher than that of oligodendroglioma (P = 0.02, Fig. 5D). Uptake in the glioblastoma lesion group (n = 8, SUV_{max} 1.95 ± 0.89) was significantly higher than that in the non-glioblastoma lesion group (n = 10, SUV_{max} 1.11 ± 0.74, P = 0.045) (Fig. 5E). The optimal cut-off value for diagnosis was 1.58, with a sensitivity of 84.6%, specificity of 75.0% and AUC of 0.76 (Fig. 5F).

In terms of tumor grade, our analysis revealed a significant difference between grades for glioma patients, including those with primary and recurrent gliomas (P = 0.047, Fig. 5G). The uptake of high-grade gliomas was higher than that of low-grade, however, the statistical difference was not found to be significant (1.64 ± 0.89 *vs.* 1.00 ± 0.70, P = 0.13, Fig. 5H). The optimal cut-off value for diagnosis was identified to be 1.12, at which point the diagnosis demonstrated a sensitivity of 72.2%, a specificity of 80.0% and an AUC of 0.73 (Fig. 5I). Similarly, when the primary glioma population was analyzed in isolation, a significant difference in SUV_{max} was observed between the different grades (grade 4 1.81 ± 0.79, grade 3 0.89 ± 0.92, grade 2 0.74 ± 0.43, P = 0.03, Fig. 5J). The uptake of high-grade gliomas was significantly higher than that of low-grade tumors (high-grade 1.59 ± 0.89, low-grade 0.74 ± 0.43, P = 0.02, Fig. 5K). The optimal cut-off value for diagnosis was determined to be 1.12, with a sensitivity of 70.6% and 100% specificity, as well as an AUC of 0.81 (Fig. 5L).

Correlation of imaging parameters and molecular features

The correlation between GRPR immunohistochemical staining results (H-score) and SUV_{max} in 19 pathological

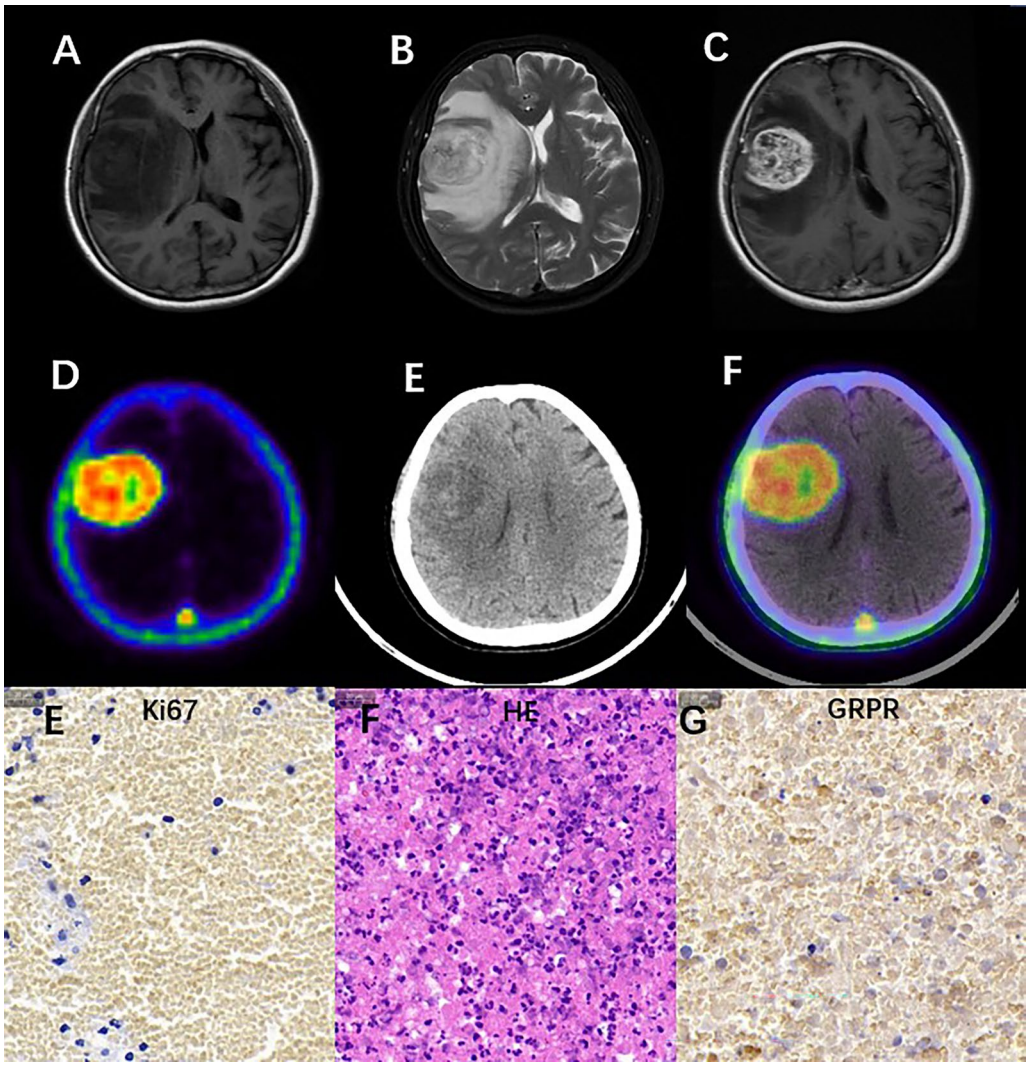

Fig. 2 A GBM lesion was seen in the right frontal lobe of a 61-year-old woman (**A** T1; **B** T2; **C** T1 + C; **D** transverse axial view of ^{68}Ga-NOTA-RM26 PET, **E** CT; **F** ^{68}Ga-NOTA-RM26 PET/CT fusion map). The SUV_{max} of the tumor was 2.34, whereas that of the contralateral brain tissue was SUV_{max} was only 0.22; **E**, **F** Ki-67 and HE staining of the tumor; **G** positive GRPR staining of the tumor

sections of 23 glioma lesions was analyzed. Spearman correlation analysis showed that there was a correlation between them ($P < 0.01$, Fig. 6). SUV_{max} didn't significantly correlate with Tumor mutation load (TMB) ($P = 0.28$) or Ki-67 ($P = 0.58$) (Fig. 6B, C). P53 alteration was found significant difference of SUV_{max} ($P = 0.03$) (Fig. 6D). No significant differences were found in other molecular alterations including IDH mutation, 1p/19q co-deletion, *CDKN2A/B* homozygous deletion, *TERT* promoter mutation, and chromosome variations including gain of chromosome 7 and loss of chromosome 10 (+7/− 10 copy number changes) (Fig. 6E–I). And no significant differences were found for *MGMT* promoter methylation, *ATRX* alteration, *Oligo2* alteration, *NeuN* alteration, *S100* alteration and *Syn* alteration (Supplementary Fig. 1).

Discussion

^{18}F-FDG is currently the most commonly used PET tracer for tumors. However, physiological glucose hypermetabolism in the brain limits its application. A number of alternative PET tracers for brain tumors are under development, including peptide receptor-targeted tracers, such as RM26, which targeting GRPR. This study demonstrates that ^{68}Ga-NOTA-RM26 is a safe and well-tolerated agent after administration. In this study, all glioma lesions showed favorable uptake of ^{68}Ga-NOTA-RM26 with a distinct tumor to background ratio. All

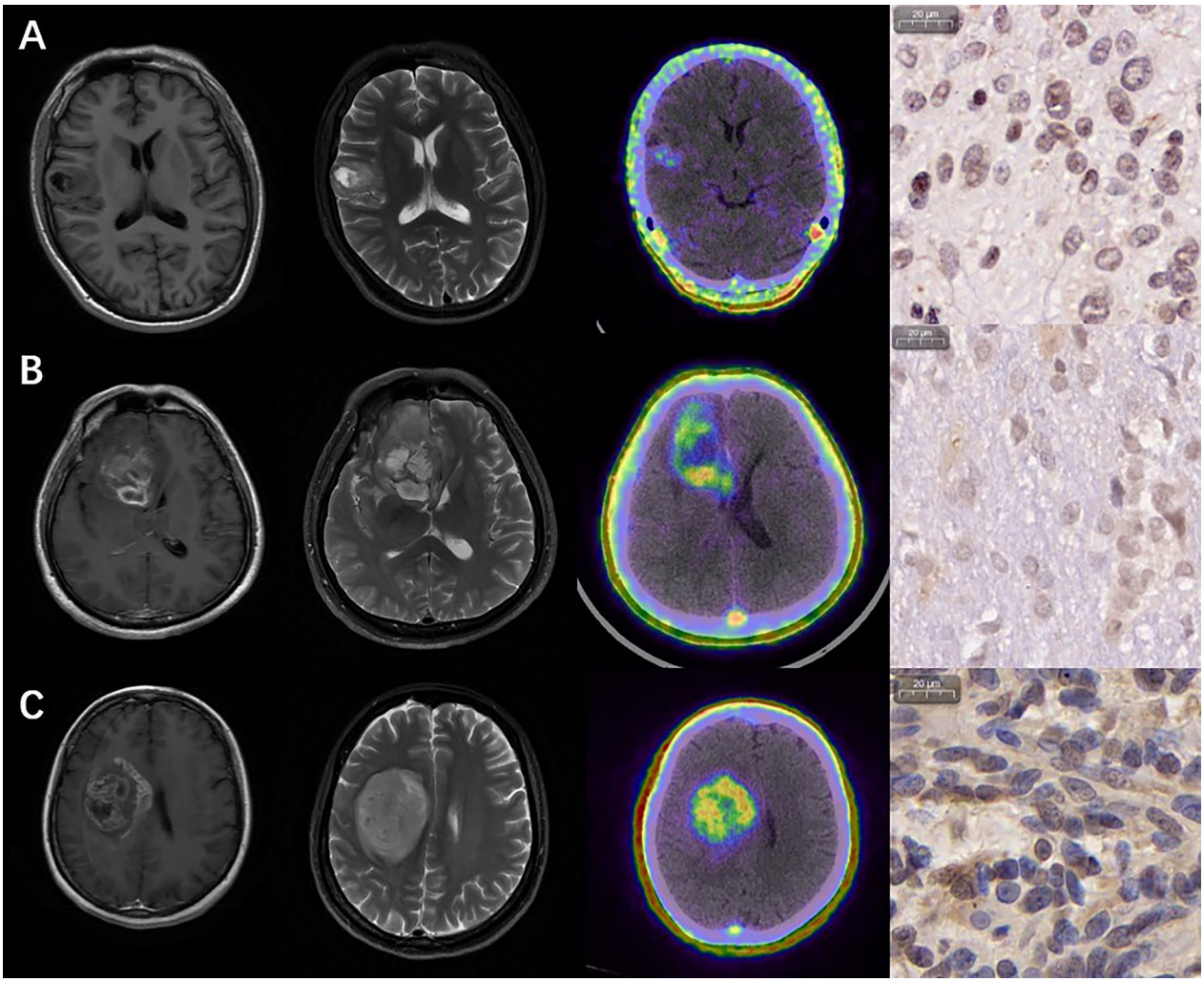

Fig. 3. ^{68}Ga-NOTA-RM26 images (left), MRI (middle) and immunohistochemically stained samples (right) of different grades of gliomas. **A** A 24-year-old male with an astrocyte, IDH mutant, WHO2-grade lesion was seen in the right frontal lobe, the SUV_{max} of the tumor was 0.58, whereas that of the contralateral brain tissue was only 0.11, and the tumor stained positively for GRPR. **B** A 49-year-old man with an oligodendrocyte, WHO grade 3 lesion in the right frontal lobe with a of 1.13 and a contralateral brain tissue SUV_{max} of 0.15, and the tumor stains positively for GRPR. **C** A 41-year-old woman with an astrocyte in the right frontal lobe, IDH mutant, WHO grade 4 lesion, with a tumor SUVmax of 1.58 and a contralateral brain tissue SUV_{max} of 0.19, and a tumor that stains positively for GRPR

glioma samples exhibited positive GRPR expression, which was consistent with the findings reported in previous pathological studies [16, 21]. A significant correlation was observed between SUV_{max} and GRPR expression, as determined by immunohistochemical staining ($P<0.01$). The imaging parameter for analysis was identified as SUV_{max} in this study. There were significant differences in the uptake values of different classifications ($P=0.045$) and grades ($P=0.03$) of primary gliomas. After the exclusion of recurrent gliomas, the difference of SUV_{max} between high-grade and low-grade gliomas was statistically significant ($P=0.02$). The uptake of recurrent grade 2 oligodendroglioma was significantly increased, possibly due to greater blood–brain barrier (BBB) disruption caused by treatment [29]. Nevertheless, the sample size is limited, and further investigation is required. Given the significant correlation between tumor types and grades in gliomas and prognosis, it is reasonable to infer that ^{68}Ga-NOTA-RM26 PET/CT may also have prognostic potential. Furthermore, this imaging agent has the potential to be employed in subsequent monitoring of treatment response.

In our study, the regions shown by PET were slightly larger than the region of enhancement in the T1+C sequence. Previous studies have shown that the T1+C range was surrounded by diffuse isolated tumor cells

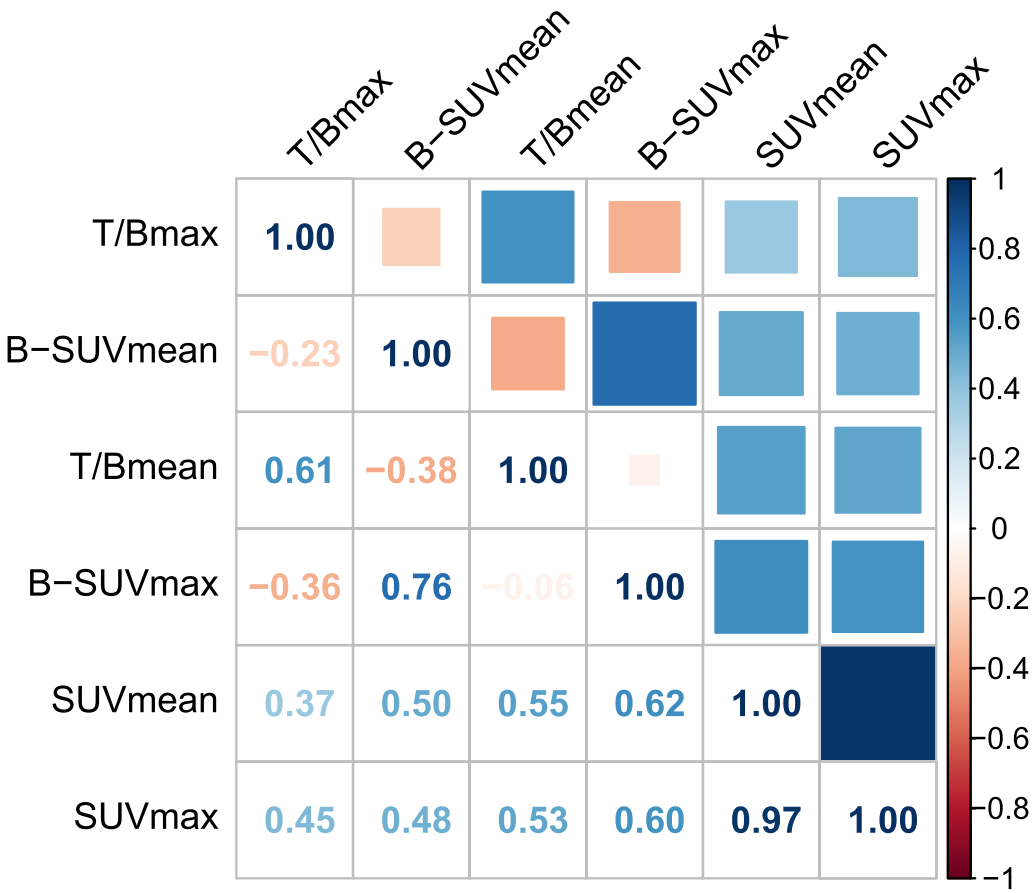

Fig. 4 Correlation between imaging parameters

that migrate into the brain [30, 31]. RANO resect group has pointed out the removal of non-contrast-enhancing tumor beyond the contrast-enhancing tumor borders may translate into additional survival benefit [32, 33]. Recent studies have shown that PET-guided tumor boundaries tend to be more accurate than MRI boundaries [34, 35], and that radiotherapy guided by PET planning tumor boundaries has a better prognosis compared to conventional MRI in small studies [36, 37]. ^{68}Ga-NOTA-RM26 has the same potential to do so. It is also important to note that the use of different radiotracers may vary to some extent, and the therapeutic efficacy of ^{68}Ga-NOTA-RM26 in determining the boundaries needs to be verified in subsequent studies. The combination of the GRPR target with intraoperative fluorescence has the potential to significantly enhance the convenience of surgical procedures and increase the resection rate. It has shown that tracer consisting of the GRPR agonist BBN linked to fluorophores was safe and effective for intraoperative tumor imaging [38]. In addition, ^{68}Ga-NOTA-RM26 PET/CT exhibited pronounced intra-tumoral heterogeneity, facilitating the investigation of intra-tumoral heterogeneity, including the spatial transcriptome [39].

Another innovative point of this study was the combination of PET/CT with molecular pathology. High GRPR expression may indicate greater likelihood of p53 mutation ($P=0.03$). Previous studies have found that in glioblastoma cell lines, GRPR knockdown leads to altered cell size, reduced proliferation and cell cycle arrest [40]. Another study showed that GRPR may play an inhibitory role on p53 function resulting in inhibition of cell cycle arrest and senescence [41]. This were consistent with our findings. The results of this study further indicated that GRPR may represent a promising target for glioma therapy. Internal irradiation with nuclides targeting peptide receptors has been the subject of extensive study and has been demonstrated to be an effective treatment for metastatic tumors [42]. As an antagonist, RM26 is less likely to produce a target effect than an agonist. It is encouraging to envisage the integration of diagnosis and treatment of gliomas. IDH-mutated gliomas generally have a better prognosis compared prognosis compared to IDH-wildtype gliomas [43]. The differences in other

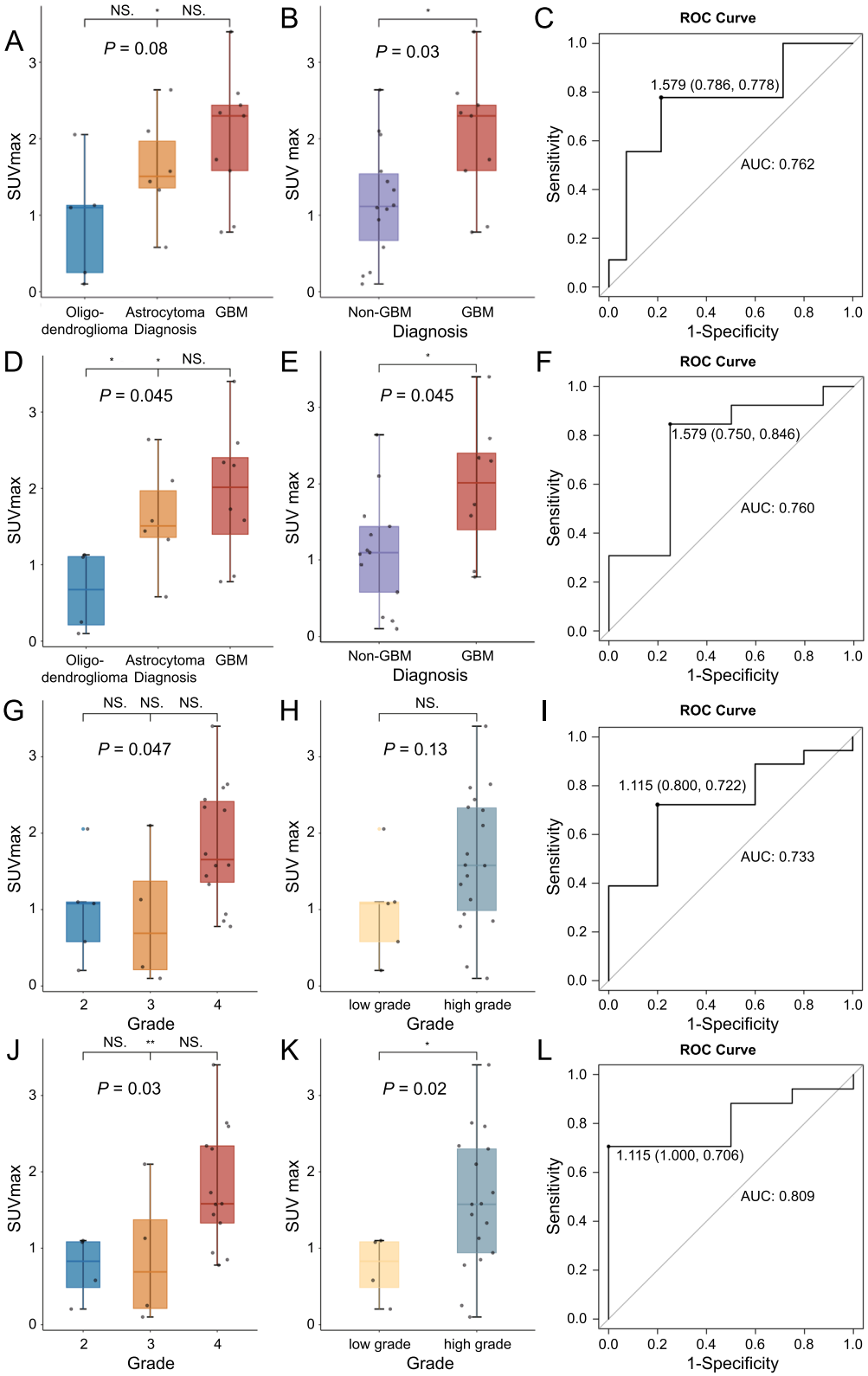

Fig. 5 Correlation between SUV_{max} and diagnosis. Correlation between SUV_{max} and glioma types for all gliomas (**A**, **B**) and primary gliomas (**D**, **E**). ROC curve for distinguishing GBM and non-GBM for all gliomas (**C**) and primary gliomas (**F**). Correlation between SUV_{max} and glioma grade for all gliomas (**J**–**H**) and primary gliomas (**J**–**K**). ROC curve for distinguishing high-grade gliomas and low-grade gliomas for all gliomas (**I**) and primary gliomas (**L**)

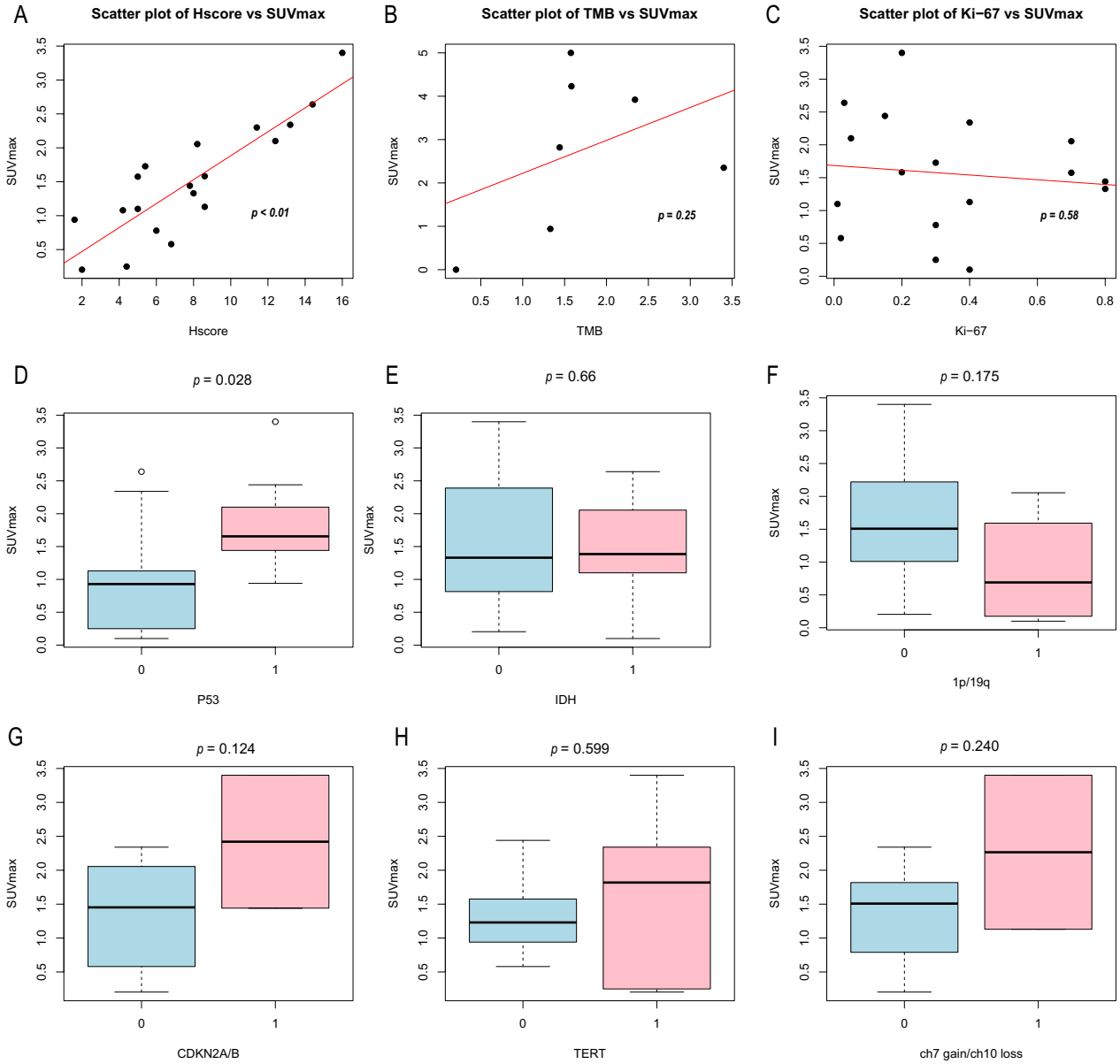

Fig. 6 Correlation between SUV_{max} and H-score (**A**), TMB (**B**), Ki-67 (**C**). Differences of SUV_{max} in P53 alteration, IDH mutation, 1p/19q co-deletion, *CDKN2A/B* homozygous deletion, *TERT* promoter mutation, and chromosome variations including gain of chromosome 7 and loss of chromosome 10 (+7/− 10 copy number changes) (**E**–**I**). 0 represents wild type and 1 represents molecular alterations

molecular alterations such as IHD mutations did not show statistical significance on PET/CT, which may be related to the small sample size. The homozygous deletion of *CDKN2A/B* is the strongest implicated independent indicator of the poor prognosis within IDH-mutant astrocytoma, and the identification of this alteration in these lower histologic grade tumors transforms their biology toward an aggressive grade 4 phenotype clinically [44]. The presence of *TERT* promoter mutations or a combination of chromosome 7 gains and 10 deletions upgraded IDH wild-type astrocytoma to glioblastoma [2, 43]. The mean SUV_{max} of them in this study were slightly higher in the mutant group than in the non-mutant group, although they did not show statistical significance. 1p/19q co-deletion is a better prognostic marker [45], with slightly lower SUV_{max} in the codeletion group compared to the wild-type group in this study, although there was no statistically significant difference.

This study also has some limitations. The number of patients included in the study was relatively limited,

and the study was conducted at a single center. Consequently, the sensitivity and specificity of the diagnosis may be subject to some degree of bias. And the limited data set made it challenging to achieve definitive positive correlations through molecular alterations and imaging characteristics, and further exploration is required to address this. Moreover, the tumor area of PET/CT and MRI showed incomplete overlap, and more findings will be found if further computer fitting and intraoperative multi-point biopsy verification are performed. In addition, the imaging parameter we used was the classic SUV_{max}, the potential for utilizing additional imaging parameters as biomarkers warrants further investigation and analysis.

Conclusions

This study is the first to demonstrate the safety and efficacy of ^{68}Ga-NOTA-RM26, a novel imaging agent with GRPR target specificity, in PET imaging of gliomas. ^{68}Ga-NOTA-RM26 PET/CT has value in the diagnostic typing and grading of gliomas. It also demonstrated that GRPR-targeted molecular imaging may be a promising modality for assessing efficacy, estimating prognosis, targeting therapy, and delineating tumors in patients with gliomas.

Abbreviations

WHO	World Health Organization
CNS	Central nervous system
MRI	Magnetic resonance imaging
PET	Positron emission tomography
^{18}F-FDG	2-^{18}F-fluoro-2-deoxyglucose
GRPR	Gastrin-releasing peptide receptor
RM26	D-Phe-Gln-Trp-Ala-Val-Gly-His-Sta-Leu-NH2
T/B ratio	Tumor-to-background ratio
SUV	Standardized uptake value
PBS	Phosphate-Buffered Saline
BSA	Bovine Serum Albumin
ANOVA	Analysis of variance
IDH	Isocitrate dehydrogenase
SUV	Standard uptake value
TMB	Tumor mutation load

Supplementary Information

The online version contains supplementary material available at https://doi.org/10.1186/s13550-025-01198-7.

Supplementary figure 1: Differences of SUV_{max} in *MGMT* promoter methylation, *ATRX* alteration , *Oligo2* alteration, *NeuN* alteration, *S100* alteration and *Syn* alteration (A-F). 0 represents wild type and 1 represents molecular alterations.

Acknowledgements

Not applicable.

Author contributions

Conception and design of the work were performed by ZZ, YW and WM. Clinical studies and data analysis were performed by YL, RW and ZZ, and pathologic analysis were performed by JC and YL. The first draft of the manuscript was written by YL and RW, and revised by ZZ, YW, JC and WM. Funding was provided by ZZ, YW and WM. All authors have approved the final manuscript.

Funding

This work was funded by the National Natural Science Foundation of China (82151302, 82272046), the National High Level Hospital Clinical Research Funding (2022-PUMCH-B-113, 2022-PUMCH-C-004, 2022-PUMCH-D-002, 2022-PUMCH-A-019), and Chinese Academy of Medical Science Innovation Fund for Medical Sciences (2021-I2M-1-014, 2021-I2M-1-016, 2022-I2M-2-002, 2022-I2M-C&T-A-008).

Availability of data and materials

The datasets used and/or analyzed during the current study are available from the corresponding author on reasonable request.

Declarations

Ethics approval and consent to participate

This study was performed in line with the principles of the Declaration of Helsinki. The study protocol was approved by the Ethics Committee of Peking Union Medical College Hospital (ZS-1103), and written informed consent was obtained from all participants.

Consent for publication

Not applicable.

Competing interests

Not applicable.

Received: 1 September 2024 Accepted: 7 January 2025
Published online: 17 January 2025

References

1. Schaff LR, Mellinghoff IK. Glioblastoma and other primary brain malignancies in adults: a review. JAMA. 2023;329:574–87. https://doi.org/10.1001/jama.2023.0023.
2. Louis DN, Perry A, Wesseling P, Brat DJ, Cree IA, Figarella-Branger D, et al. The 2021 WHO classification of tumors of the central nervous system: a summary. Neuro Oncol. 2021;23:1231–51. https://doi.org/10.1093/neuonc/noab106.
3. Stupp R, Mason WP, Bent MJ, Weller M, Fisher B, Taphoorn MJB, et al. Radiotherapy plus concomitant and adjuvant temozolomide for glioblastoma. N Engl J Med. 2005;352:987–96. https://doi.org/10.1056/NEJMoa043330.
4. Stupp R, Taillibert S, Kanner A, Read W, Steinberg DM, Lhermitte B, et al. Effect of tumor-treating fields plus maintenance temozolomide vs maintenance temozolomide alone on survival in patients with glioblastoma: a randomized clinical trial. JAMA. 2017;318:2306–16. https://doi.org/10.1001/jama.2017.18718.
5. Juweid ME, Cheson BD. Positron-emission tomography and assessment of cancer therapy. N Engl J Med. 2006;354:496–507. https://doi.org/10.1056/NEJMra050276.
6. di Chiro G, Brooks RA, Patronas NJ, Bairamian D, Kornblith PL, Smith BH, et al. Issues in the in vivo measurement of glucose metabolism of human central nervous system tumors. Ann Neurol. 1984;15:138–46. https://doi.org/10.1002/ana.410150727.
7. Arora G, Sharma P, Sharma A, Mishra AK, Hazari PP, Biswas A, et al. 99mTc-methionine hybrid SPECT/CT for detection of recurrent glioma: comparison with 18F-FDG PET/CT and contrast-enhanced MRI. Clin Nucl Med. 2018;43:e132–8. https://doi.org/10.1097/rlu.0000000000002036.
8. Unterrainer M, Schweisthal F, Suchorska B, Wenter V, Schmid-Tannwald C, Fendler WP, et al. Serial 18F-FET PET imaging of primarily 18F-FET-negative glioma: does it make sense? J Nucl Med. 2016;57:1177–82. https://doi.org/10.2967/jnumed.115.171033.

9. Maurer GD, Brucker DP, Stoffels G, Filipski K, Filss CP, Mottaghy FM, et al. (18)F-FET PET imaging in differentiating glioma progression from treatment-related changes: a single-center experience. J Nucl Med. 2020;61:505–11. https://doi.org/10.2967/jnumed.119.234757.
10. Langen K-J, Galldiks N. Update on amino acid PET of brain tumours. Curr Opin Neurol. 2018;31:354–61. https://doi.org/10.1097/wco.0000000000000574.
11. Cicone F, Filss CP, Minniti G, Rossi-Espagnet C, Papa A, Scaringi C, et al. Volumetric assessment of recurrent or progressive gliomas: comparison between F-DOPA PET and perfusion-weighted MRI. Eur J Nucl Med Mol Imaging. 2015;42:905–15. https://doi.org/10.1007/s00259-015-3018-5.
12. García Vicente AM, Pérez-Beteta J, Bosque JJ, Soriano Castrejón ÁM, Pérez-García VM. Multiple and diffuse gliomas by 18F-fluorocholine PET/CT: two sides of the same coin. Clin Nucl Med. 2022;47:e457–65. https://doi.org/10.1097/rlu.0000000000004145.
13. Brahm CG, den Hollander MW, Enting RH, de Groot JC, Solouki AM, den Dunnen WFA, et al. Serial FLT PET imaging to discriminate between true progression and pseudoprogression in patients with newly diagnosed glioblastoma: a long-term follow-up study. Eur J Nucl Med Mol Imaging. 2018;45:2404–12. https://doi.org/10.1007/s00259-018-4090-4.
14. Albert NL, Galldiks N, Ellingson BM, van den Bent MJ, Chang SM, Cicone F, et al. PET-based response assessment criteria for diffuse gliomas (PET RANO 10): a report of the RANO group. Lancet Oncol. 2024;25:e29–41. https://doi.org/10.1016/S1470-2045(23)00525-9.
15. Sharif TR, Luo W, Sharif M. Functional expression of bombesin receptor in most adult and pediatric human glioblastoma cell lines; role in mitogenesis and in stimulating the mitogen-activated protein kinase pathway. Mol Cell Endocrinol. 1997;130:119–30. https://doi.org/10.1016/s0303-7207(97)00080-4.
16. Flores DG, Meurer L, Uberti AF, Macedo BR, Lenz G, Brunetto AL, et al. Gastrin-releasing peptide receptor content in human glioma and normal brain. Brain Res Bull. 2010;82:95–8. https://doi.org/10.1016/j.brainresbull.2010.02.014.
17. Moody TW, Mahmoud S, Staley J, Naldini L, Cirillo D, South V, et al. Human glioblastoma cell lines have neuropeptide receptors for bombesin/gastrin-releasing peptide. J Mol Neurosci. 1989;1:235–42.
18. Pinski J, Schally AV, Halmos G, Szepeshazi K, Groot K. Somatostatin analogues and bombesin/gastrin-releasing peptide antagonist RC-3095 inhibit the growth of human glioblastomas in vitro and in vivo. Cancer Res. 1994;54:5895–901.
19. de Oliveira MS, Cechim G, Braganhol E, Santos DG, Meurer L, de Castro CG, et al. Anti-proliferative effect of the gastrin-release peptide receptor antagonist RC-3095 plus temozolomide in experimental glioblastoma models. J Neurooncol. 2009;93:191–201. https://doi.org/10.1007/s11060-008-9775-2.
20. Breeman WAP, Verbruggen AM. The 68Ge/68Ga generator has high potential, but when can we use 68Ga-labelled tracers in clinical routine? Eur J Nucl Med Mol Imaging. 2007;34:978–81. https://doi.org/10.1007/s00259-007-0387-4.
21. Zhang J, Li D, Lang L, Zhu Z, Wang L, Wu P, et al. 68Ga-NOTA-Aca-BBN(7–14) PET/CT in healthy volunteers and glioma patients. J Nucl Med. 2016;57:9–14. https://doi.org/10.2967/jnumed.115.165316.
22. Bodei L, Ferrari M, Nunn A, Llull J, Cremonesi M, Martano L, et al. Lu-177-AMBA bombesin analogue in hormone refractory prostate cancer patients: a phase I escalation study with single-cycle administrations. In: European journal of nuclear medicine and molecular imaging. SPRINGER 233 SPRING STREET, NEW YORK, NY 10013 USA; 2007. p. S221-S.
23. Cescato R, Maina T, Nock B, Nikolopoulou A, Charalambidis D, Piccand V, et al. Bombesin receptor antagonists may be preferable to agonists for tumor targeting. J Nucl Med. 2008;49:318–26. https://doi.org/10.2967/jnumed.107.045054.
24. Varasteh Z, Velikyan I, Lindeberg G, Sörensen J, Larhed M, Sandström M, et al. Synthesis and characterization of a high-affinity NOTA-conjugated bombesin antagonist for GRPR-targeted tumor imaging. Bioconjug Chem. 2013;24:1144–53. https://doi.org/10.1021/bc300659k.
25. Mansi R, Wang X, Forrer F, Kneifel S, Tamma M-L, Waser B, et al. Evaluation of a 1,4,7,10-tetraazacyclododecane-1,4,7,10-tetraacetic acid-conjugated bombesin-based radioantagonist for the labeling with single-photon emission computed tomography, positron emission tomography, and therapeutic radionuclides. Clin Cancer Res. 2009;15:5240–9. https://doi.org/10.1158/1078-0432.CCR-08-3145.
26. Zhang J, Niu G, Fan X, Lang L, Hou G, Chen L, et al. PET using a GRPR antagonist (68)Ga-RM26 in healthy volunteers and prostate cancer patients. J Nucl Med. 2018;59:922–8. https://doi.org/10.2967/jnumed.117.198929.
27. Zang J, Mao F, Wang H, Zhang J, Liu Q, Peng L, et al. 68Ga-NOTA-RM26 PET/CT in the evaluation of breast cancer: a pilot prospective study. Clin Nucl Med. 2018;43:663–9. https://doi.org/10.1097/rlu.0000000000002209.
28. Loose D, Signore A, Staelens L, Bulcke KV, Vermeersch H, Dierckx RA, et al. 123I-Interleukin-2 uptake in squamous cell carcinoma of the head and neck carcinoma. Eur J Nucl Med Mol Imaging. 2008;35:281–6. https://doi.org/10.1007/s00259-007-0609-9.
29. Hart E, Odé Z, Derieppe MPP, Groenink L, Heymans MW, Otten R, et al. Blood–brain barrier permeability following conventional photon radiotherapy—a systematic review and meta-analysis of clinical and preclinical studies. Clin Transl Radiat Oncol. 2022;35:44–55. https://doi.org/10.1016/j.ctro.2022.04.013.
30. Claes A, Idema AJ, Wesseling P. Diffuse glioma growth: a guerilla war. Acta Neuropathol. 2007;114:443–58. https://doi.org/10.1007/s00401-007-0293-7.
31. Lemée J-M, Clavreul A, Menei P. Intratumoral heterogeneity in glioblastoma: don't forget the peritumoral brain zone. Neuro Oncol. 2015;17:1322–32. https://doi.org/10.1093/neuonc/nov119.
32. Karschnia P, Young JS, Dono A, Häni L, Sciortino T, Bruno F, et al. Prognostic validation of a new classification system for extent of resection in glioblastoma: a report of the RANO resect group. Neuro Oncol. 2022;25:940–54. https://doi.org/10.1093/neuonc/noac193.
33. Karschnia P, Gerritsen JKW, Teske N, Cahill DP, Jakola AS, van den Bent M, et al. The oncological role of resection in newly diagnosed diffuse adult-type glioma defined by the WHO 2021 classification: a review by the RANO resect group. Lancet Oncol. 2024;25:e404–19. https://doi.org/10.1016/S1470-2045(24)00130-X.
34. Lohmann P, Stavrinou P, Lipke K, Bauer EK, Ceccon G, Werner J-M, et al. FET PET reveals considerable spatial differences in tumour burden compared to conventional MRI in newly diagnosed glioblastoma. Eur J Nucl Med Mol Imaging. 2019;46:591–602. https://doi.org/10.1007/s00259-018-4188-8.
35. Dissaux G, Dissaux B, Kabbaj OE, Gujral DM, Pradier O, Salaün P-Y, et al. Radiotherapy target volume definition in newly diagnosed high grade glioma using 18F-FET PET imaging and multiparametric perfusion MRI: a prospective study (IMAGG). Radiother Oncol. 2020;150:164–71. https://doi.org/10.1016/j.radonc.2020.06.025.
36. Harat M, Blok M, Miechowicz I, Wiatrowska I, Makarewicz K, Małkowski B. Safety and efficacy of irradiation boost based on 18F-FET-PET in patients with newly diagnosed glioblastoma. Clin Cancer Res. 2022;28:3011–20. https://doi.org/10.1158/1078-0432.CCR-22-0171.
37. Laack NN, Pafundi D, Anderson SK, Kaufmann T, Lowe V, Hunt C, et al. Initial results of a phase 2 trial of 18F-DOPA PET-guided dose-escalated radiation therapy for glioblastoma. Int J Radiat Oncol Biol Phys. 2021;110:1383–95. https://doi.org/10.1016/j.ijrobp.2021.03.032.
38. Li D, Zhang J, Chi C, Xiao X, Wang J, Lang L, et al. First-in-human study of PET and optical dual-modality image-guided surgery in glioblastoma using (68)Ga-IRDye800CW-BBN. Theranostics. 2018;8:2508–20. https://doi.org/10.7150/thno.25599.
39. Harat M, Rakowska J, Harat M, Szylberg T, Furtak J, Miechowicz I, et al. Combining amino acid PET and MRI imaging increases accuracy to define malignant areas in adult glioma. Nat Commun. 2023;14:4572. https://doi.org/10.1038/s41467-023-39731-8.
40. Qiao J, Kang J, Ishola TA, Rychahou PG, Evers BM, Chung DH. Gastrin-releasing peptide receptor silencing suppresses the tumorigenesis and metastatic potential of neuroblastoma. Proc Natl Acad Sci USA. 2008;105:12891–6. https://doi.org/10.1073/pnas.0711861105.
41. Menegotto PR, da Costa Lopez PL, Souza BK, de Farias CB, Filippi-Chiela EC, Vieira IA, et al. Gastrin-releasing peptide receptor knockdown induces senescence in glioblastoma cells. Mol Neurobiol. 2017;54:888–94. https://doi.org/10.1007/s12035-016-9696-6.
42. Sartor O, Bono J, Chi KN, Fizazi K, Herrmann K, Rahbar K, et al. Lutetium-177-PSMA-617 for metastatic castration-resistant prostate cancer. N Engl J Med. 2021;385:1091–103. https://doi.org/10.1056/NEJMoa2107322.
43. Śledzińska P, Bebyn MG, Furtak J, Kowalewski J, Lewandowska MA. Prognostic and predictive biomarkers in gliomas. Int J Mol Sci. 2021;22:10373. https://doi.org/10.3390/ijms221910373.

44. Fortin Ensign SP, Jenkins RB, Giannini C, Sarkaria JN, Galanis E, Kizilbash SH. Translational significance of CDKN2A/B homozygous deletion in isocitrate dehydrogenase-mutant astrocytoma. Neuro Oncol. 2022;25:28–36. https://doi.org/10.1093/neuonc/noac205.
45. Familiari PLP, Picotti V, Palmieri M, Pesce A, Carosi G, Relucenti M, Nottola S, Gianno F, Minasi S, Antonelli M, et al. Role of 1p/19q codeletion in diffuse low-grade glioma tumour prognosis. Anticancer Res. 2023;43:2659–70. https://doi.org/10.21873/anticanres.16432.

Publisher's Note